# Supplementary materials for Mechanistic Insights into Signal Generation and Probing Depth in Photothermal-Based Atomic Force Microscopy-Infrared (AFM-IR)

Yide Zhang,[†,‡] Margaux Petay,[†] Alexandre Dazzi,[¶] Bernhard Lendl,[†] and Georg Ramer[*,†,‡]

†*Institute of Chemical Technologies and Analytics, TU Wien, Vienna, 1060, Austria*

‡*Christian Doppler Laboratory for Advanced Mid-Infrared Laser Spectroscopy in (Bio-)process Analytics, TU Wien, Vienna, 1060, Austria*

¶*Institut de Chimie Physique, Université Paris-Saclay - CNRS UMR8000, Orsay, 91400, France*

E-mail: georg.ramer@tuwien.ac.at

## Photothermal Modeling

To model generalized sample scenarios, we consider a three-layer geometry (Fig. S1) in which an undering layer of thickness $h$ lies beneath an covering layer of thickness $h_1$, supported by a substrate treated as a semi-infinite thermal sink due to its high thermal diffusivity. We simplify heat conduction to a one-dimensional (1D) problem defined over the finite domain $0 \leq z \leq (h + h_1)$, where $z = 0$ denotes the air/sample interface and the absorbing layer occupies $z \in [h_1, h_1 + h]$. For simplicity, the thermal properties of the two polymer layers

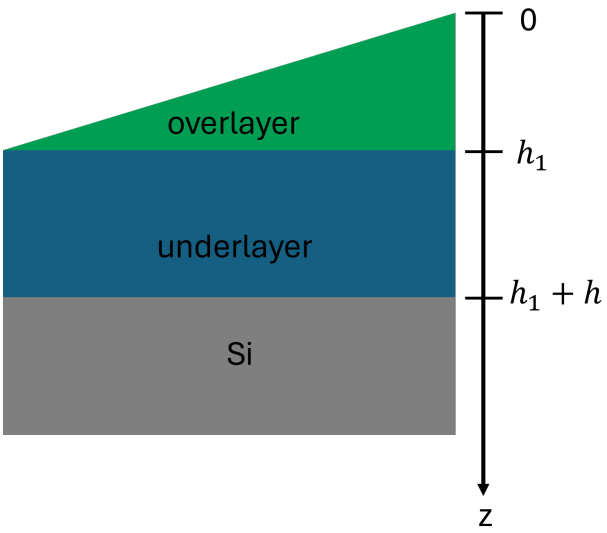


Figure S1: Schematic of the layered sample geometry used in this study. The layered sample consists of two layers, an overlayer of varying thickness (0 to $h_1$) and an underlying layer extending from $h_1$to $h+h_1$, deposited on a silicon substrate treated as a semi-infinite thermal sink.

are averaged to form an effective medium.

## Laser absorption and heat generation

For times $t > 0$, the absorber is illuminated by an excitation laser, leading to internal volumetric heat generation described by $g(z,t)$. Assuming Beer–Lambert attenuation within the absorbing layer, we write

$$g(z,t) = \begin{cases} \mu_a \dfrac{P}{A} e^{-\beta z}, & 0 \le z < h_1 \quad \text{(overlayer absorption)}, \\ \mu_a \dfrac{P}{A} e^{-\beta (z-h_1)}, & h_1 \le z < h_1 + h \quad \text{(underlayer absorption)}, \\ 0, & z \ge h_1 + h, \end{cases} \tag{S1}$$

where $\mu_a$ is the optical absorption coefficient, $P$ is the excitation laser power, $A$ is the optical fluence area, and $\beta$ is the optical decay coefficient.

The mathematical formulation of the 1D heat-conduction problem is

$$\frac{\partial^2 T(z,t)}{\partial z^2} + \frac{g(z,t)}{\kappa} = \frac{1}{\alpha}\frac{\partial T(z,t)}{\partial t} \quad \text{in} \quad 0 \leq z \leq h + h_1 \quad , \; t > 0, \tag{S2}$$

where $\kappa$ is the thermal conductivity and $\alpha$ is the thermal diffusivity.

Initial and boundary conditions are

$$\begin{aligned} &\text{BC1}: \quad \left.\frac{\partial T}{\partial z}\right|_{z=0} = 0 \quad \text{(air is thermally insulating)}, \\ &\text{BC2}: \quad T(z,t)\big|_{z=h+h_1} = 0 \quad \text{(substrate acts as a heat sink)}, \\ &\text{IC}: \quad T(z,0) = F(z) \quad \text{(initial temperature)}. \end{aligned} \tag{S3}$$

To determine the desired Green's function, we consider the homogeneous version of the problem over the same region:

$$\frac{\partial^2 \Psi(z,t)}{\partial z^2} = \frac{1}{\alpha}\frac{\partial \Psi(z,t)}{\partial t} \quad \text{in} \quad 0 \leq z \leq h + h_1 \quad , \; t > 0. \tag{S4}$$

Assuming separation of variables,

$$\Psi(z,t) = Z(z)\Gamma(t), \tag{S5}$$

substitution into Eq. (S4) yields

$$\frac{1}{Z}\frac{d^2 Z}{dz^2} = \frac{1}{\alpha\Gamma}\frac{d\Gamma}{dt} = -\lambda^2, \tag{S6}$$

where $\lambda$ is the separation constant. The temporal solution is

$$\Gamma(t) = C_1 e^{-\alpha\lambda^2 t}, \tag{S7}$$

and the spatial solution is

$$Z(z) = C_2 \cos(\lambda z) + C_3 \sin(\lambda z). \tag{S8}$$

Applying BC1 gives $C_3 = 0$, hence

$$Z(z) = C_2 \cos(\lambda z). \tag{S9}$$

Applying BC2 yields

$$C_2 \cos\big(\lambda(h + h_1)\big) = 0, \tag{S10}$$

which gives the eigenvalues

$$\lambda_n = \frac{(2n+1)\pi}{2(h+h_1)}, \quad n = 0, 1, 2, \ldots \tag{S11}$$

Summing over all eigenmodes gives

$$\Psi(z,t) = \sum_{n=0}^{\infty} c_n \cos(\lambda_n z)\, e^{-\alpha \lambda_n^2 t}, \tag{S12}$$

where $c_n = C_1 C_2$. Applying the initial condition yields the Fourier expansion

$$F(z) = \sum_{n=0}^{\infty} c_n \cos(\lambda_n z). \tag{S13}$$

Multiplying both sides by $\cos(\lambda_i z)$ and integrating over the domain $[0, h + h_1]$ gives

$$c_n = \frac{2}{h+h_1} \int_0^{h+h_1} F(z') \cos(\lambda_n z')\, dz'. \tag{S14}$$

Substitution of Eq. (S14) into Eq. (S12) yields

$$\Psi(z,t) = \frac{2}{h+h_1}\int_0^{h+h_1} F(z')\sum_{n=0}^{\infty} e^{-\alpha\lambda_n^2 t}\cos(\lambda_n z)\cos(\lambda_n z')\,dz'. \tag{S15}$$

Comparing with the Green's function representation,

$$\Psi(z,t) = \int_0^{h+h_1} F(z')\,G(z,t\,|\,z',0)\,dz', \tag{S16}$$

we identify

$$G(z,t\,|\,z',0) = \frac{2}{h+h_1}\sum_{n=0}^{\infty} e^{-\alpha\lambda_n^2 t}\cos(\lambda_n z)\cos(\lambda_n z'). \tag{S17}$$

Replacing $t$ by $(t-\tau)$ gives the full Green's function

$$G(z,t\,|\,z',\tau) = \frac{2}{h+h_1}\sum_{n=0}^{\infty} e^{-\alpha\lambda_n^2 (t-\tau)}\cos(\lambda_n z)\cos(\lambda_n z'), \qquad t>\tau. \tag{S18}$$

The solution of the non-homogeneous problem in Eq. (S2) in terms of the above Green's function (without prescribed boundary temperature) is given by.[S1] Considering the case of underlayer-absorption $g(z,t)$ is applied only within the absorbing layer $z \in [h_1,\, h_1+h]$.

$$\begin{aligned} T(z,t) = &\int_{z'=0}^{\infty} G(z,t|z',\tau)|_{\tau=0} F(z')dz' \\ &+ \frac{\alpha}{\kappa}\int_{\tau=0}^{t}\int_{z'=h_1}^{h} G(z,t|z',\tau)g(z',\tau)e^{-\beta(z'-h_1)}dz' \\ &+ \alpha\sum_{1}^{N}\left\{\int_{\tau=0}^{t} G(z,t|z',\tau)|_{z'=z_i}\frac{1}{k}f_i(\tau)d\tau\right\} \end{aligned} \tag{S19}$$

In our case, the medium is initially at equilibrium with no temperature variation ($F(z)=0$) and no inhomogeneous boundary temperature ($f_i$) is prescribed, so the temperature field describes the temperature rise. The solution therefore reduces to

$$T(z,t) = \frac{\alpha}{\kappa}\int_0^t\int_{h_1}^{h_1+h} G(z,t\,|\,z',\tau)\,g(z',\tau)\,dz'\,d\tau, \tag{S20}$$

where the spatial integral is restricted to the absorbing layer $z' \in [h_1,\, h_1 + h]$.

Substituting Eq. (S18) into Eq. (S20) yields

$$\begin{aligned} T(z,t) &= \frac{\alpha}{\kappa} \int_0^t \int_{h_1}^{h_1+h} \frac{2}{h+h_1} \sum_{n=0}^{\infty} e^{-\alpha\lambda_n^2 (t-\tau)} \cos(\lambda_n z) \cos(\lambda_n z')\, g(z',\tau)\, dz'\, d\tau \\ &= \frac{2\alpha\mu_a P}{\kappa(h+h_1)A_f} \sum_{n=0}^{\infty} \cos(\lambda_n z)\, I_n\, \Gamma(t), \end{aligned} \tag{S21}$$

where the spatial factor $I_n$ is

$$I_n = \int_{h_1}^{h_1+h} \cos(\lambda_n z')\, e^{-\beta(z'-h_1)}\, dz'. \tag{S22}$$

Let $u = z' - h_1$ (so $du = dz'$). Then Eq. (S22) becomes

$$I_n = \int_0^h \cos\big(\lambda_n (u+h_1)\big) e^{-\beta u}\, du. \tag{S23}$$

Rewriting the Eq. S23 in terms of $u$:

$$I_n = \int_{u=0}^{h} cos\lambda_n (u+h_1) e^{-\beta u} du = \underbrace{\cos\lambda_n h_1 \int_{u=0}^{h} cos\lambda_n u e^{-\beta u} du}_{\mathrm{I}_1} \underbrace{- \sin\lambda_n h_1 \int_{u=0}^{h} sin\lambda_n u e^{-\beta u} du}_{\mathrm{I}_2} \tag{S24}$$

$$I_1 = \cos\lambda_n h_1 \int_{u=0}^{h} cos\lambda_n u e^{-\beta u} du = \cos\lambda_n h_1 \Big(\frac{\lambda_n \sin\lambda_n h - \beta\cos\lambda_n h}{\lambda_n^2+\beta^2} e^{-\beta h} + \frac{\beta}{\lambda_n^2+\beta^2}\Big) \tag{S25}$$

$$I_2 = -\sin\lambda_n h_1 \int_{u=0}^{h} sin\lambda_n u e^{-\beta u} du = \sin\lambda_n h_1 \Big(\frac{\lambda_n \cos\lambda_n h + \beta\sin\lambda_n h}{\lambda_n^2+\beta^2} e^{-\beta h} - \frac{\lambda_n}{\lambda_n^2+\beta^2}\Big) \tag{S26}$$

$$
\begin{aligned}
I_n &= I_1 + I_2 \\
&= \frac{\lambda_n(\cos\lambda_n h_1 \sin\lambda_n h + \sin\lambda_n h_1 \cos\lambda_n h) + \beta(\sin\lambda_n h_1 \sin\lambda_n h - \cos\lambda_n h_1 \cos\lambda_n h)}{\lambda_n^2 + \beta^2} e^{-\beta h} \\
&+ \frac{\beta\cos\lambda_n h_1 - \lambda_n \sin\lambda_n h_1}{\lambda_n^2 + \beta^2} \\
&= \frac{\lambda_n(\sin\lambda_n(h_1+h)e^{-\beta h} - \sin\lambda_n h_1) + \beta(\cos\lambda_n h_1 - \cos\lambda_n(h_1+h)e^{-\beta h})}{\lambda_n^2 + \beta^2}
\end{aligned}
\tag{S27}
$$

Take the solution of $\lambda_n$ from Equation S11, Equation S27 can be further simplified to

$$
I_n = \frac{\lambda_n(e^{-\beta h}(-1)^n - \sin\lambda_n h_1) + \beta\cos\lambda_n h_1}{\lambda_n^2 + \beta^2} \tag{S28}
$$

The time-dependent function $\Gamma(t)$ is defined as

$$
\Gamma(t) = \int_0^t e^{-\alpha\lambda_n^2(t-\tau)}\, \Pi\left(\frac{\tau}{t_p}\right) d\tau, \tag{S29}
$$

where $\Pi(\tau/t_p)$ is a rectangular pulse of width $t_p$.

This expression represents the convolution of the exponential decay function

$$
g(t) = e^{-\alpha\lambda_n^2 t} u(t), \qquad u(t) = \begin{cases} 0 & \text{for } t < 0, \\ 1 & \text{for } t \geq 0, \end{cases} \tag{S30}
$$

and the rectangular pulse $\Pi(t/t_p)$:

$$
\Gamma(t) = g(t) * \Pi\left(\frac{t}{t_p}\right). \tag{S31}
$$

## Frequency domain response

### Single pulse

Taking the Fourier transform gives

$$G(f) = \mathcal{F}\{g(t)\} = \frac{1}{\alpha\lambda_n^2 + i2\pi f}, \tag{S32}$$

and

$$\Pi(f) = \mathcal{F}\left\{\Pi\left(\frac{t}{t_p}\right)\right\} = t_p\ \mathrm{sinc}(\pi f t_p)\, e^{-i\pi f t_p}. \tag{S33}$$

Using the convolution theorem,

$$\Gamma(f) = G(f)\Pi(f) = \frac{t_p\ \mathrm{sinc}(\pi f t_p)}{\alpha\lambda_n^2 + i2\pi f}\, e^{-i\pi f t_p}. \tag{S34}$$

### Pulse train

For a periodic pulse train with repetition rate $f_{\mathrm{rep}}$, the total response can be written as a superposition of time-shifted single-pulse responses,

$$\Gamma_{\mathrm{train}}(t) = \sum_{m=-\infty}^{\infty} \Gamma\left(t - \frac{m}{f_{\mathrm{rep}}}\right). \tag{S35}$$

This expression is appropriate when the system fully relaxes between pulses (i.e., negligible thermal accumulation). Equivalently, $\Gamma_{\mathrm{train}}(t)$ can be expressed as a convolution of $\Gamma(t)$ with a Dirac comb,

$$\Gamma_{\mathrm{train}}(t) = \Gamma(t) * \sum_{m=-\infty}^{\infty} \delta\left(t - \frac{m}{f_{\mathrm{rep}}}\right). \tag{S36}$$

In the frequency domain, the Dirac comb maps to a discrete set of harmonics at integer multiples of $f_{\mathrm{rep}}$, giving

$$\Gamma_{\mathrm{train}}(f) = \Gamma(f) \sum_{m=-\infty}^{\infty} \delta(f - m f_{\mathrm{rep}}) \tag{S37}$$

$$= \sum_{m=-\infty}^{\infty} \delta(f - m f_{\mathrm{rep}})\ \Gamma(m f_{\mathrm{rep}})\,. \tag{S38}$$

Using the single-pulse spectrum derived above,

$$\Gamma(m f_{\mathrm{rep}}) = \frac{t_p\ \mathrm{sinc}(\pi m f_{\mathrm{rep}} t_p)}{\alpha \lambda_n^2 + i 2\pi m f_{\mathrm{rep}}}\, e^{-i\pi m f_{\mathrm{rep}} t_p}, \tag{S39}$$

the pulse-train spectrum becomes

$$\Gamma_{\mathrm{train}}(f) = \sum_{m=-\infty}^{\infty} \frac{t_p\ \mathrm{sinc}(\pi m f_{\mathrm{rep}} t_p)}{\alpha \lambda_n^2 + i 2\pi m f_{\mathrm{rep}}}\, e^{-i\pi m f_{\mathrm{rep}} t_p}\, \delta(f - m f_{\mathrm{rep}})\,. \tag{S40}$$

## Thermal expansion of the sample

We use a quasi-static approximation, neglecting inertial effects under slow thermal loading. The mechanical response is assumed to follow the temperature field instantaneously, without elastic wave propagation. The 1D thermoelastic equation is

$$(\lambda + 2\mu)\frac{\partial^2 u}{\partial z^2} - \gamma \frac{\partial T}{\partial z} = 0, \tag{S41}$$

where $\gamma = (3\lambda + 2\mu)\alpha_T$. The Lamé constants are

$$\lambda = \frac{E\nu}{(1+\nu)(1-2\nu)}, \qquad \mu = \frac{E}{2(1+\nu)}, \tag{S42}$$

with Young's modulus $E$, Poisson's ratio $\nu$, and linear thermal expansion coefficient $\alpha_T$.

Rearranging Eq. (S41) gives

$$\frac{\partial^2 u}{\partial z^2} = \frac{\gamma}{\lambda + 2\mu}\frac{\partial T}{\partial z} = \frac{1+\nu}{1-\nu}\alpha_T \frac{\partial T}{\partial z}. \tag{S43}$$

At a free surface ($z = 0$), the normal stress vanishes,

$$\sigma_{zz} = 0, \tag{S44}$$

and the constitutive relation yields

$$\sigma_{zz} = (\lambda + 2\mu)\frac{\partial u}{\partial z} - \gamma T. \tag{S45}$$

Thus, the free-surface boundary condition becomes

$$(\lambda + 2\mu)\left.\frac{\partial u}{\partial z}\right|_{z=0} - \gamma T(0, f) = 0. \tag{S46}$$

The resulting surface displacement can be expressed as

$$u(0, f) = \frac{1+\nu}{1-\nu}\alpha_T \int T(z, f)\, dz, \tag{S47}$$

with the integration constant determined by the chosen reference (e.g., $u = 0$ at the thermally fixed boundary).

By supplementing Eq. S21, S28, S40 into above equation, we have

$$\begin{aligned} u(0, f) =& \frac{2\alpha\mu_a P}{\kappa(h + h_1)A_f} \sum_{n=0}^{\infty} \frac{\lambda_n(e^{-\beta h}(-1)^n - \sin\lambda_n h_1) + \beta\cos\lambda_n h_1}{\lambda_n(\lambda_n^2 + \beta^2)} \\ & \sum_{m=-\infty}^{\infty} \frac{t_p\ \mathrm{sinc}(\pi m f_{\mathrm{rep}} t_p)}{\alpha\lambda_n^2 + i2\pi m f_{\mathrm{rep}}}\, e^{-i\pi m f_{\mathrm{rep}} t_p}\, \delta(f - m f_{\mathrm{rep}})\,. \end{aligned} \tag{S48}$$

# Cantilever dynamics

The key component of an AFM setup is the cantilever, whose length, width, and material properties directly determine its mechanical resonance frequencies and spring constant. These parameters govern the force sensitivity, response time, and suitability for different imaging modes.

The most commonly used cantilever geometry is beam-shaped and can be modeled using Euler–Bernoulli beam theory:[S2]

$$EI\frac{\partial^4 z(x,t)}{\partial x^4} + \eta\rho A\frac{\partial z(x,t)}{\partial t} + \rho A\frac{\partial^2 z(x,t)}{\partial t^2} = 0, \tag{S49}$$

where $z(x,t)$ is the transverse displacement, $E$ is Young's modulus, $I = WH^3/12$ is the area moment of inertia, $\rho$ is the density, $A = WH$ is the cross-sectional area, and $\eta$ is a phenomenological damping coefficient accounting for both structural and environmental dissipation.[S3]

We assume a modal expansion of the form

$$z(x,t) = \phi_n(x)\, q_n(t), \tag{S50}$$

where $\phi_n(x)$ is the mode shape and $q_n(t)$ is the modal amplitude. Substitution into Eq. (S49) and separation of variables yields the spatial eigenvalue problem

$$\frac{d^4\phi_n}{dx^4} = k_n^4\phi_n, \tag{S51}$$

with $k_n^4 = \rho A\omega_{n,0}^2/(EI)$.

For a clamped–free beam, the boundary conditions lead to the characteristic equation

$$\cos(k_n L)\cosh(k_n L) + 1 = 0, \tag{S52}$$

which determines the free resonance frequencies $\omega_{n,0}$. The corresponding mode shapes are

$$\phi_n(x) = C\Big[(\cosh k_n x - \cos k_n x) - \frac{\cosh k_n L + \cos k_n L}{\sinh k_n L + \sin k_n L}(\sinh k_n x - \sin k_n x)\Big], \tag{S53}$$

where the normalization constant $C$ is chosen such that $\phi_n(L) = 1$.

The effective modal mass is then

$$m_{\mathrm{eff},n} = \int_0^L \rho A \phi_n^2(x)\, dx. \tag{S54}$$

Photothermal expansion of the sample is modeled as an impulsive force $I_{\mathrm{imp}}\delta(t)$ acting on the cantilever.[S4] The resulting equation of motion is

$$\ddot{q}_n + 2\zeta\omega_n\dot{q}_n + \omega_n^2 q_n = \frac{I_{\mathrm{imp}}}{m_{\mathrm{eff},n}}\,\delta(t), \tag{S55}$$

where $\zeta$ is the damping ratio and $\omega_n = \sqrt{(k_0 + k_c)/m_{\mathrm{eff},n}}$ is the contact resonance frequency.

With initial conditions $\dot{q}_n(0) = I_{\mathrm{imp}}/m_{\mathrm{eff},n}$ and $q_n(0) = 0$, the solution is

$$q_n(t) = \frac{I_{\mathrm{imp}}}{m_{\mathrm{eff},n}\omega_d} e^{-\zeta\omega_n t}\sin(\omega_d t), \tag{S56}$$

where $\omega_d = \omega_n\sqrt{1-\zeta^2}$ denotes the damped angular frequency.[S5]

The frequency-domain signal $Q_n(\omega)$ is obtained via the Fourier transform:

$$Q_n(\omega) = \int_0^\infty q_n(t)e^{-i\omega t}\, dt = \frac{I_{\mathrm{imp}}}{m_{\mathrm{eff},n}}\frac{1}{\omega_n^2 - \omega^2 + 2i\zeta\omega_n\omega}. \tag{S57}$$

The AFM-IR amplitude at frequency $\omega$ is therefore

$$|Q_n(\omega)| = \frac{I_{\mathrm{imp}}}{m_{\mathrm{eff},n}}\frac{1}{\sqrt{(\omega_n^2 - \omega^2)^2 + (2\zeta\omega_n\omega)^2}}. \tag{S58}$$

Considering the tip–sample contact, the photothermal excitation is modeled as an im-

pulsive force, whose impulse is given by

$$I_{\mathrm{imp}} = \int_0^\infty F_{\mathrm{th}}(t)\, dt \approx k_c \Delta u, \tag{S59}$$

where $k_c$ is the contact stiffness and $\Delta u$ is the thermally induced surface expansion.

The resulting contact resonance frequency is

$$\omega_n = \sqrt{\frac{k_0 + k_c}{m_{\mathrm{eff},n}}}, \tag{S60}$$

where $k_0$ is the free cantilever stiffness.

Evaluating Eq. (S58) at the contact resonance $\omega = \omega_n$ and assuming weak damping ($\zeta \ll 1$), the oscillation amplitude becomes

$$Q_n(\omega_n) = \frac{k_c \Delta u}{2\zeta m_{\mathrm{eff},n} \omega_n}. \tag{S61}$$

While Eq. (S61) predicts the frequency dependence of the contact-resonant amplitude in the weakly damped, linear regime, the absolute amplitude generally deviates from this simple scaling in practical AFM-IR measurements due to several effects not captured by the model:

- **Contact stiffness variations.** The effective contact stiffness $k_c$ can vary significantly with sample material, local mechanical heterogeneity, and operating conditions (e.g., setpoint or indentation depth), directly rescaling the measured amplitude.

- **Torsional and twisting effects during scanning.** Lateral friction forces can induce cantilever torsion and modify the effective mechanical response (including the apparent stiffness and mode shape), leading to systematic deviations from the purely vertical, linear oscillator model.

- **Nonlinear response at large amplitudes.** At sufficiently high excitation ampli-

tudes, the cantilever–contact dynamics can depart from the linear approximation due to amplitude-dependent stiffness or damping, resulting in deviations from the predicted resonant scaling.

As a consequence, the model primarily constrains the frequency-dependent scaling of the AFM-IR amplitude, while the absolute amplitude prefactor remains uncertain and experiment dependent. We therefore perform the analysis using normalized amplitudes, which suppresses poorly controlled parameters such as $k_c$, friction-induced torsion, and other setup-dependent factors, while preserving the predicted frequency dependence.

Table S1: The thermal, mechanical and thermo-mechanical properties of PMMA and PS are listed below. [S6,S7]

| Property* | PMMA | PS |
|---|---|---|
| coefficient of thermal expansion (1/K) | $193.6 \times 10^{-6}$ | $153 \times 10^{-6}$ |
| thermal conductivity (W/(m· K)) | 0.192 | 0.131 |
| density ($kg/m^3$) | 1190 | 1050 |
| specific heat capacity at constant pressure (J/(kg·K)) | 1420 | 1131 |
| specific heat capacity at constant volume (J/(kg·K)) | - | 1100 |
| Young's modulus (GPa) | 2.4 | 2.6 |
| Strain transmission speed (m/s) | - | 2050 |
| Poisson's ratio | 0.37 | 0.36 |
| effective viscosity ($Pa \cdot s$) | – | $7 \times 10^4$ |

*These values are treated as exact numbers for the purpose of simulations.

# References


[S1] Hahn, D. W.; Özişik, M. N. *Heat conduction*, 3rd ed.; Wiley: Hoboken, NJ, 2012.

[S2] Mendels, D.-A.; Lowe, M.; Cuenat, A.; Cain, M. G.; Vallejo, E.; Ellis, D.; Mendels, F. Dynamic properties of AFM cantilevers and the calibration of their spring constants. *Journal of Micromechanics and Microengineering* **2006**, *16*, 1720–1733.

[S3] Rabe, U.; Turner, J.; Arnold, W. Analysis of the high-frequency response of atomic

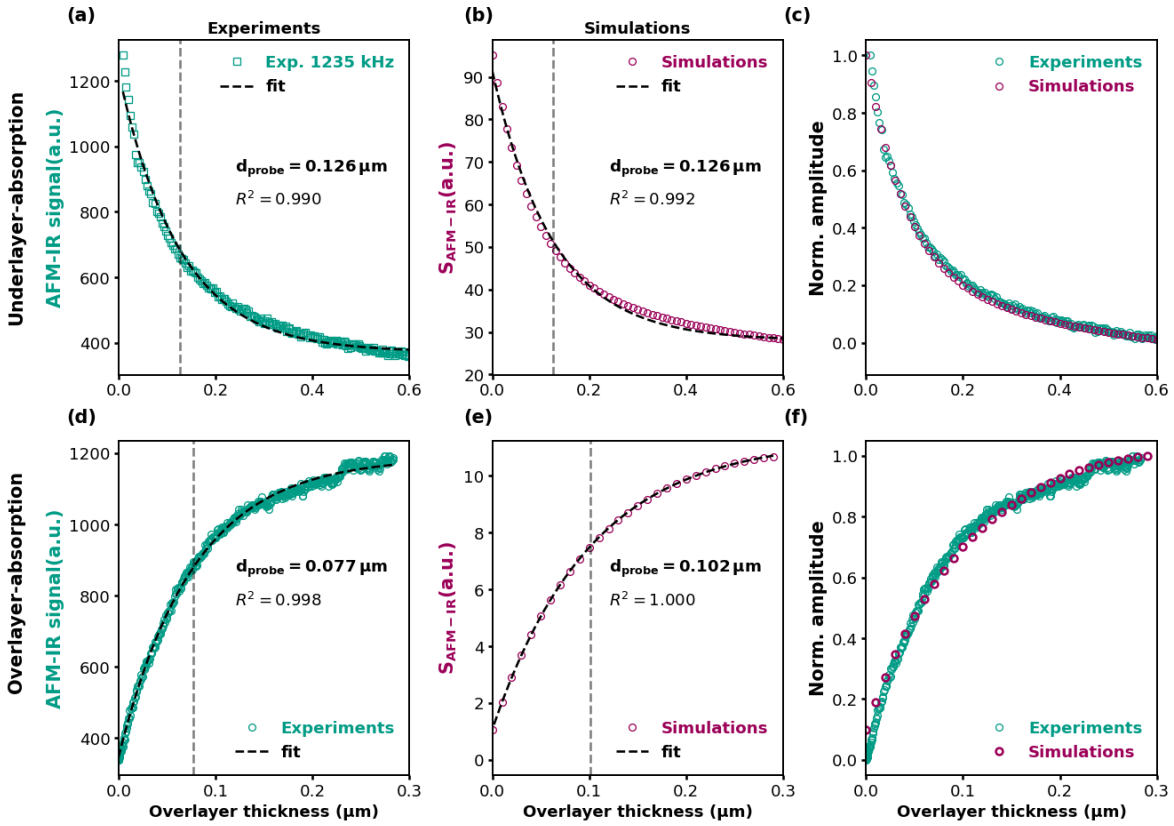


Figure S2: Comparison between experimental and simulated AFM-IR signals at a modulation frequency of 1230 kHz for underlayer- and overlayer-absorption configurations. (a,d) Experimental AFM-IR signal as a function of overlayer thickness for underlayer absorption (a) and overlayer absorption (d). (b,e) Corresponding simulated AFM-IR signals with consideration of both $\beta$ and $\gamma$. (c,f) Normalized amplitudes comparing experimental and simulated results. Dashed lines indicate exponential fits used to extract an effective probing depth $d_{\mathrm{probe}}$. For the underlayer-absorption case, the signal decay is fitted using $s(h_1) = d_1 + d_2 e^{-d_3 h_1}$, whereas for the overlayer-absorption case, the signal growth and saturation are fitted using $s(h_1) = d_1 + d_2 \left(1 - e^{-d_3 h_1}\right)$.

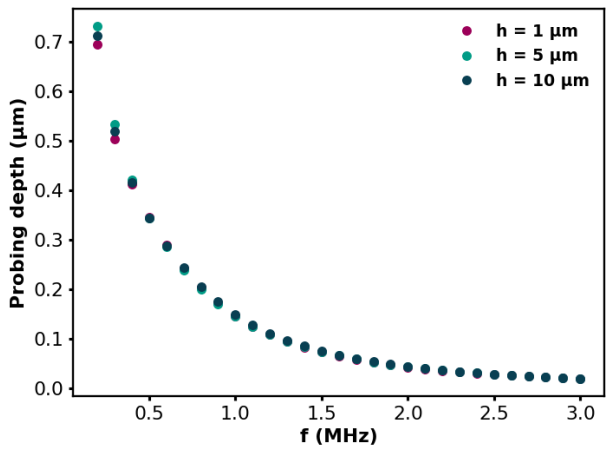


Figure S3: Probing depth as a function of modulation frequency for PMMA layers with thicknesses of 1 µm, 5 µm, and 10 µm.

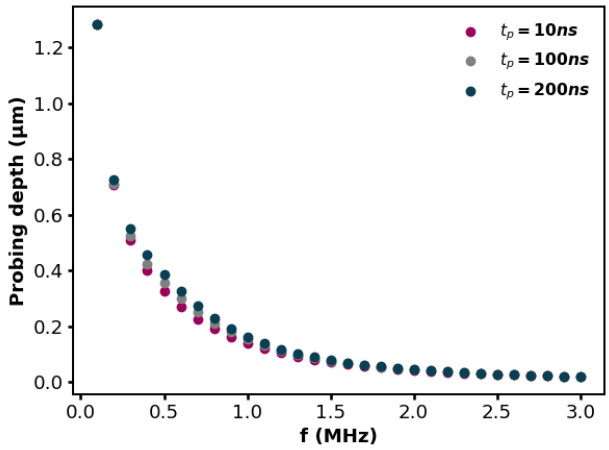


Figure S4: Frequency dependence of the AFM-IR probing depth. Extracted probing depth as a function of modulation frequency for three excitation pulse widths ($t_p$ = 10 ns, 100 ns and 200 ns). The probing depth decreases monotonically with increasing frequency and shows only a weak dependence on pulse width over the explored range.

force microscope cantilevers. *Applied Physics A: Materials Science & Processing* **1998**, *66*, S277–S282.

[S4] Dazzi, A.; Glotin, F.; Carminati, R. Theory of infrared nanospectroscopy by photothermal induced resonance. *Journal of Applied Physics* **2010**, *107*, 124519.

[S5] Bao, M.-H. *Handbook of Sensors and Actuators*; Elsevier, 2000; Vol. 8; pp 23–88.

[S6] Zhang, Y.; Yilmaz, U.; Lukasievicz, G. V. B.; O'Faolain, L.; Lendl, B.; Ramer, G. An analytical model of label-free nanoscale chemical imaging reveals avenues toward improved spatial resolution and sensitivity. *Proceedings of the National Academy of Sciences* **2025**, *122*, e2403079122.

[S7] Ashby, M. F. *Materials and the Environment*; Elsevier, 2013; pp 459–595.